High-fidelity gate operations with the coupled nuclear and electron spins of a nitrogen-vacancy center in diamond

Mark S. Everitt,[1,*] Simon Devitt,[1] W. J. Munro,[1,2] and Kae Nemoto[1,†]

[1]*National Institute of Informatics, 2-1-2 Hitotsubashi, Chiyoda-ku, Tokyo 101-8430, Japan*

[2]*NTT Basic Research Laboratories, NTT Corporation, 3-1 Morinosato-Wakamiya, Atsugi, Kanagawa 243-0198, Japan*

(Received 8 August 2012; revised manuscript received 14 March 2014; published 15 May 2014)

In this article we investigate the dynamics of a single negatively charged nitrogen-vacancy center (NV^-) coupled to the spin of the nucleus of a 15-nitrogen atom and show that high-speed, high-fidelity gate operations are possible without the need for complicated composite pulse sequences. These operations include both the electron and nuclear spin rotations, as well as an entangling gate between them. These are the primitive gates one will need within a quantum node of a distributed communication network.

DOI: 10.1103/PhysRevA.89.052317 PACS number(s): 03.67.Lx, 76.30.Mi, 61.72.jn

I. INTRODUCTION

The quest to build quantum repeaters and computers and to do communication with quantum processes has been one of the most ambitious and difficult technological challenges of the 21st century so far. There have been many physical systems identified as potential candidates [1]. One that has enjoyed significant recent attention has been diamond. Diamond has many exceptional properties [2–4]; it is the hardest known material, is chemically inert, possesses a broad optical transparency window, and can accommodate a large variety of optically active color centers. Of these color centers, the negatively charged nitrogen vacancy (NV^-) center [5–7] has attracted particular interest [8]. It exhibits properties that make it useful for a wide range of interesting applications, including quantum information devices as well as sensitive probes of magnetic fields [9–12] and biomarking tracking [13–16]. It offers a quantum-mechanical system that is remarkably isolated from the environment, "trapped" in a carbon lattice giving it excellent potential for quantum-information processing-based applications [17–20].

The NV^- center is composed of an electron spin (spin 1) and at least one nuclear spin coupled by the hyperfine interaction [5–7]. It is straightforward to manipulate both the NV^- electron and nuclear degrees of freedom [21–25], and the long lived nuclear spin [26] makes it attractive as a quantum memory [20]. Furthermore, previous studies have shown that remote centers may be coupled by using light [27]. Indeed, heralded entanglement between solid-state qubits separated by three meters has been shown [28]. Together, these features give us a tantalizing indication of a physical system with which to build quantum information processors, provided high-precision operations are possible [29–34].

In this article we investigate the potential of a single NV^- center to act with high fidelity as a node in a hybrid distributed quantum computer [29–33]. Our considerations will focus on the NV^- center's electron spin with a coupling via the hyperfine interaction to a single ^{15}N nuclear spin. The choice of ^{15}N is motivated by the simpler nuclear energy level structure (spin $\frac{1}{2}$), which is a natural qubit, compared with that of ^{14}N (spin 1) or ^{13}C which has also been extensively studied [22,28] but would involve controlling a tripartite system. We will show that it should be possible to enact a high-fidelity universal set of quantum logic gates, with error probabilities below fault-tolerant thresholds for topological error correction ($\sim$0.6% [35]), between the electron and nuclear spins with a static magnetic field [36]. These gates consist of a hyperfine derived controlled-phase gate, driven polarized microwave single-qubit rotations on the NV^- center, and driven hyperfine mediated single-qubit rotations on the nuclear spin. Such operations are primitives for any distributed communications network. Entanglement between nodes can be accomplished by using optical photons that can be coupled to the electron spins [28]. The necessity to design high-fidelity gates under reasonable theoretical and experimental assumptions is driven by the need to have available simple and fast control sequences that, in principal, can deliver fidelities of 99.9% or higher so that once experimental fabrication and control error are taken into account and refined, the resulting system can still satisfy threshold criterion for fault-tolerant computation and communication.

The paper is structured as follows: We begin in Sec. II by defining our basic Hamiltonian process and the adoption of a rotating frame. We also discuss the critical physical parameters such as the relaxation and dephasing times of the electron and nuclear spins. Section III introduces the natural entangling gate between the electron and nuclear spin, while Secs. IV and V show how electron- and nuclear-spin rotations can be achieved, respectively, with high fidelity. Section VII shows how these basic operations can be used to build larger quantum circuits while Sec. VIII presents a concluding discussion.

II. THE SYSTEM HAMILTONIAN

Our system under consideration here consists of a single $^{15}NV^-$ center whose ^3A ground-state energy levels we illustrate in Fig. 1. The NV^- is made up of an electron spin-1 system and a nitrogen-15 nuclear spin. As the electron spin consists of three levels we must choose a pair of levels to embed the electron qubit in ($|0\rangle_e$,$|+1\rangle_e$ or $|0\rangle_e$,$|-1\rangle_e$). The nuclear spin from the nitrogen is naturally a spin-$\frac{1}{2}$ system. We describe

*mark.s.everitt@gmail.com
†nemoto@nii.ac.jp

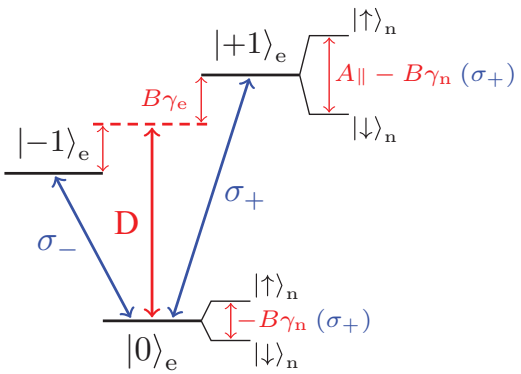

FIG. 1. (Color online) Schematic energy-level diagram of the ground-state energy manifold of an NV^- center. By setting a magnetic field such that $B\gamma_e < D$, a transition for the electron of the same circular polarization as that of the nucleus is chosen. The levels $|0\rangle_e$ and $|+1\rangle_e$ of the electron are chosen for the electron qubit (with the obvious mapping), and for the nucleus $|\uparrow\rangle_n \to |1\rangle$ and $|\downarrow\rangle_n \to |0\rangle$.

our system with the Hamiltonian $H = H_0 + H_S + H_{HF} + H_D$, where

$$H_0 = \hbar D S_z^2 + \hbar B\gamma_e S_z - \hbar B\gamma_n I_z, \tag{1}$$

$$H_S = \hbar\frac{E}{2}(S_+^2 + S_-^2), \tag{2}$$

$$H_{HF} = \hbar A_\parallel S_z I_z + \frac{1}{2}\hbar A_\perp (S_+ I_- + S_- I_+), \tag{3}$$

$$H_D = \hbar\Omega_0 \cos(\omega t + \phi)\left(S_x - \frac{\gamma_n}{\gamma_e} I_x\right), \tag{4}$$

with S_x, S_y, and S_z being the usual spin-1 operators [$S_+ = \sqrt{2}(|0\rangle_e\langle -1|_e + |+1\rangle_e\langle 0|_e)$, $S_- = S_+^\dagger$] and I_x, I_y, and I_z being the nuclear spin-$\frac{1}{2}$ operators ($I_+ = |\uparrow\rangle_n\langle\downarrow|_n$, $I_- = |\downarrow\rangle_n\langle\uparrow|_n$). The uncoupled system is given by the Hamiltonian terms $H_0 + H_S$, where the first term in H_0 is a zero-field splitting of magnitude $D/(2\pi) = 2.87$ GHz [37]. The second term is the splitting of the three electron levels determined by the magnetic field B aligned with the NV axis and the electron gyromagnetic ratio $\gamma_e = \mu_B g_e$ where $\mu_B/h = 14.0$ MHz mT^{-1} and $g_e = 2.00$. The last term in H_0 is the splitting of the two level nuclear levels determined by the magnetic field B and the nuclear gyromagnetic ratio $\gamma_n = \mu_N g_n$ with the nuclear magneton $\mu_N/h = 7.63$ kHz mT^{-1} and the nuclear g factor $g_n = -0.566$. The second term in our uncoupled system H_S represents a strain-induced splitting between the $|\pm 1\rangle_e$, where $E \sim 1-10$ MHz is typical (7 MHz is assumed here). The hyperfine coupling H_{HF} between the electron and nuclear spins is composed of a phase gate with $A_\parallel/(2\pi) = 3.03$ MHz parallel to the NV^- axis and an exchange part with $A_\perp/(2\pi) = 3.65$ MHz perpendicular to it. The exchange component of hyperfine interaction moves an excitation between the electron and nuclear spin systems and has its resonance at

$$B_{ex} = \frac{A_\parallel/2 \mp D}{\gamma_e \pm \gamma_n} \approx \mp 102\ \mathrm{mT},$$

with Lorentzian width [38]

$$B_{FWHM} = \frac{2\sqrt{2}A_\perp}{\gamma_n + \gamma_e} \approx 0.368\ \mathrm{mT}.$$

Finally, H_D is an electromagnetic driving term, with a magnitude on the electron (nucleus) determined by the gyromagnetic ratio γ_e (γ_n), and Ω_0 is the amplitude of the applied electromagnetic drive field of frequency ω and phase ϕ.

Before moving forward to examine various gate operations we need to examine the physical and coherence properties of our system. Beginning with the electron spin, the type of synthesis used to create the diamond crystal and temperature have a significant effect on the relaxation time T_1 time of the electron spin. At temperatures $T > 200$ K, Jarmola *et al.* [39] reported that high-pressure, high-temperature (HPHT) and chemical-vapor-deposition (CVD) samples showed the same T_1 time within a factor of 2. However, for lower temperatures the relaxation time can dramatically increase. For instance, with CVD samples the T_1 time could increase by almost five orders of magnitude (to 100 s) when the temperature is decreased below 80 K. This seems to strongly indicate that we want to work with a CVD diamond at moderate temperatures (4–80 K). Furthermore, the relaxation time is also increased when a small but nonzero (20 mT) external magnetic field is applied. As we describe in detail in the next section, this regime of magnetic field is preferable to control the hyperfine coupling with respect to the error-correction protocols. Applying a magnetic field allows us to split the $|\pm 1\rangle_e$ levels. Next, the dephasing time T_2 is also highly dependent on the type of diamond sample used and especially on the concentration of P1 centers (and other impurities). Electronic spin coherence times T_2^* of 90 μs and $T_2 \sim 2$ ms have been observed in isotopically purified diamond [10,40,41]. By using dynamic decoupling techniques, T_2 times as long as 0.6 s have been demonstrated in an ensemble [42]. The coherences properties of the nuclear spins can exceed 0.25 s [43].

III. THE ENTANGLING GATE

Before we begin examining gate operations we need to specify how we encode a qubit within the electron spin. In this case we choose the electron spin computational basis 0 and 1 to be $|0\rangle_e$ and $|+1\rangle_e$, respectively. The $|-1\rangle_e$ state should never be occupied and, if it is, it will be considered a leakage event. Now the hyperfine interaction between the electron and nuclear spins provides a route to entangling the spins without resorting to driving fields or varying the magnetic fields dynamically. In the case of no driving field, the interaction-picture Hamiltonian reduces to

$$\bar{H} = \hbar A_\parallel S_z I_z + \hbar\Big(E|+1\rangle_e\langle -1|_e\, e^{i2B\gamma_e t} + \frac{A_\perp}{\sqrt{2}} I_-[e^{i\Delta_+ t}|+1\rangle_e\langle 0|_e + e^{-i\Delta_- t}|0\rangle_e\langle -1|_e] + \mathrm{H.c.}\Big), \tag{5}$$

where $\hbar A_\parallel S_z I_z$ is a natural entangling gate (a controlled-phase gate), and $\Delta_\pm = D \pm B\gamma_e \pm B\gamma_n$. However, the strain-induced splitting is obviously problematic, since it provides a transition out of the computational basis of the system.

The resonances for this strain interaction occur when $B = \pm\frac{A_\parallel}{2\gamma_e}$ (positive for the nucleus is in the $|\downarrow\rangle_n$ state, and negative for the $|\uparrow\rangle_n$ state) with full width at half maximum $B_{\rm FWHM} = 2E/\gamma_e$. For a strain-induced splitting $E < 10$ MHz, the width is $B_{\rm FWHM} < 1$ mT approximately centered at 0 T. Eliminating this leakage effect is possible by choosing $B \gg E/\gamma_e$, which occurs when $B \sim 20$ mT. In such a case the strain term gives a small dispersive interaction of the form $\bar{H}_{\rm S,dis} = \frac{\hbar E^2}{2B\gamma_e}[|+1\rangle_e\langle+1|_e - |-1\rangle_e\langle-1|_e]$. When nuclear spins are facilitated as quantum memory, the exchange component is generally used for the state transfer between the electron and the nuclear spins. However, with the exchange coupling, the errors induced with this component are more problematic than ones with the control phase coupling. At the choice of $B \sim 20$ mT we are also far off resonance with the exchange component of hyperfine interaction, and so its contribution is in terms of a small dispersive shift.

In these regimes we will have negligible exchange population between the electron spins states, and so long as we start our electron spin in its qubit subspace $\{|0\rangle_e, |+1\rangle_e\}$, we can neglect the $|-1\rangle_e$ state. This means we can write the entangling operation in the $\{|0\rangle_e, |+1\rangle_e\}$ subspace as

$$\begin{aligned}\bar{H} = &\left(\hbar A_\parallel + \frac{\hbar A_\perp^2}{2\Delta_+}\right)|+1\rangle_e\langle+1|_e I_z \\ &- \left(\frac{\hbar A_\perp^2}{2\Delta_+} + \frac{\hbar A_\perp^2}{2\Delta_-}\right)|0\rangle_e\langle 0|_e I_z \\ &+ \left(\frac{\hbar E^2}{2B\gamma_e} - \frac{\hbar A_\perp^2}{4\Delta_+}\right)|+1\rangle_e\langle+1|_e \\ &- \left(\frac{\hbar A_\perp^2}{4\Delta_+} - \frac{\hbar A_\perp^2}{4\Delta_-}\right)|0\rangle_e\langle 0|_e, \end{aligned} \tag{6}$$

which includes level shifts [44] due to the strain-induced splitting and the perpendicular hyperfine interaction. To lowest order, this gives an interaction of the form

$$\bar{H} \approx \frac{\hbar A_\parallel}{2}|1\rangle_e\langle 1|_e \sigma_z^n. \tag{7}$$

The interaction is equivalent to a controlled-phase gate within a single qubit z rotation on the electron, as shown in Fig. 2. For instance, an ideal input state to create a maximally entangled pair is $|+\rangle_e|+\rangle_n \equiv \frac{1}{2}[|0\rangle_e|0\rangle_n + |0\rangle_e|1\rangle_n + |+1\rangle_e|0\rangle_n + |+1\rangle_e|1\rangle_n]$, which can be created from the ground state $|0\rangle_e|0\rangle_n$ by electron and nuclear spin rotations [45]. The gate time is determined by $A_\parallel$, which gives a time of $t_{CZ} = \pi/A_\parallel \approx 165$ ns. However, considering Eq. (6), we notice that there

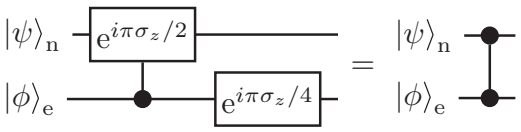

FIG. 2. Quantum circuit showing the equivalence between the hyperfine interaction and a controlled-phase gate. The interaction provided by the hyperfine Hamiltonian (the controlled gate on the left) is locally equivalent to a controlled Z (CZ) gate. As the single-qubit operation on the electron commutes with the controlled gate, it may appear on either side of it.

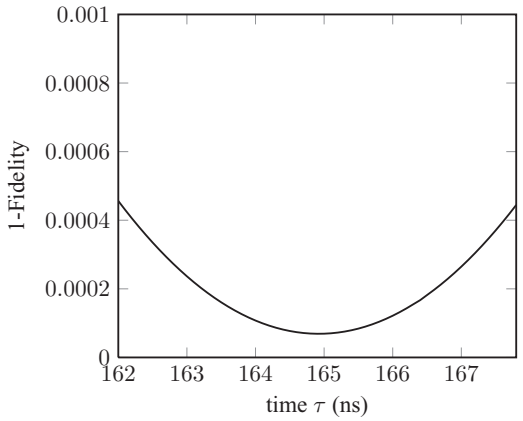

FIG. 3. Simulation illustrating the probability of error (1-Fidelity) of the CZ gate when applied to an initial electron nuclear spin state $|+\rangle_e|+\rangle_n$ to generate a maximally entangled Bell state.

are second-order terms which could be important effecting the fidelity of this gate operation. Hence we perform a simulation using the full Hamiltonian (1) but with the driving turned off. This is depicted in Fig. 3 and shows that a high-fidelity gate in principle can be achieved (with error rate $p_{\rm error} < 0.0001$). The fidelity is limited not in this case by the decoherence properties of the NV^- centers (more explicitly T_2^* of the electron spin as it can be as long as 90 μs) but by the strain and $A_\perp$ components of the hyperfine interaction. These effects could in principle be corrected by appropriate single-qubit operations on the electron and nuclear spins. Even without such corrections, a high-fidelity gate is possible when one has a long T_2^* for the electron spin. Finally, our simulations indicate for this gate that the leakage rate to the $|-1\rangle_e$ state is exceedingly small.

IV. ELECTRON ROTATIONS

For quantum-information applications we need to be able to perform well-defined single-qubit gates, including the Pauli operations X, Y, Z, the Hadamard gate H, the phase gate S, and the $\pi/8$ gate T. These can be achieved by using either free system evolution or driven electron-spin rotations.

Rotations on the electron spin can be implemented by using a microwave driving field perpendicular to the NV^- axis without the same drive also affecting the nuclear spin. This assumption is safe, since the gyromagnetic ratio of the electron is ~6500 times larger than that of the nucleus, and the microwave driving field is far off resonance with it. However, we need to be careful that the field used to drive the $|0\rangle_e \leftrightarrow |+1\rangle_e$ transition does not also drive the $|0\rangle_e \leftrightarrow |-1\rangle_e$ transition. This is true when

$$\frac{\Omega_0}{2\sqrt{2}} \ll \min[2B\gamma_e, 2D], \tag{8}$$

which is equivalent to the statement that the coupling factor of the drive field to the electron is much less than the detuning between the transition that we want to drive and the transition that we do not want to drive. The limit has been demonstrated experimentally [46] and becomes apparent at attempted cycle times of a few tens of nanoseconds. In Figs. 4(a)–4(d) we show the error probability (1-Fidelity) for a

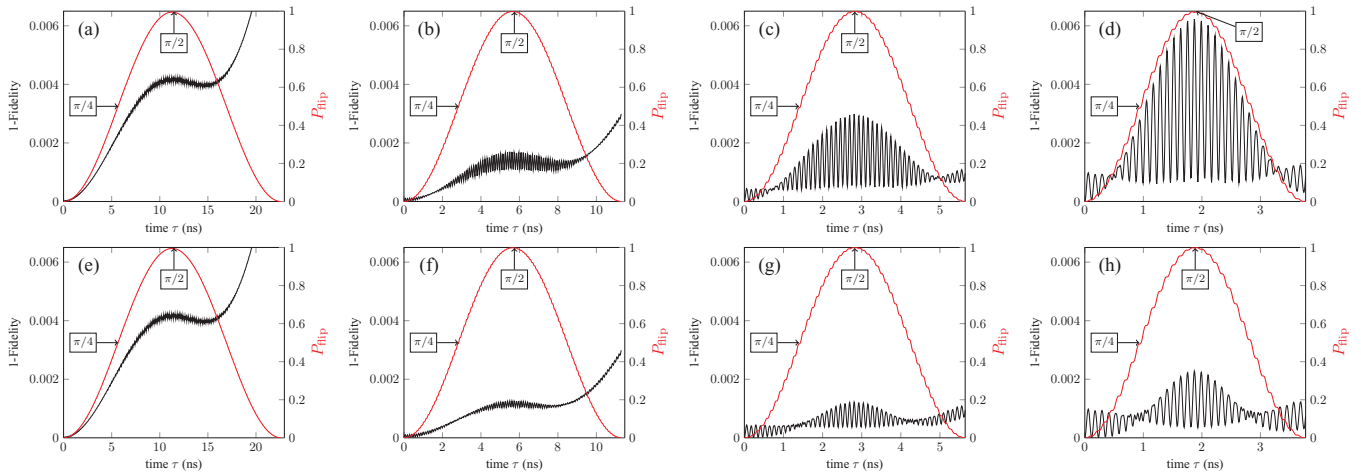

FIG. 4. (Color online) Simulation illustrating the probability of error (1-Fidelity) of the driven system compared to the ideal electron-spin-qubit rotations versus rotation time. An unpolarized microwave field is used in panels (a)–(d) while a polarized field is used in panels (e)–(h). Four different drive amplitudes were considered: 62.5 MHz for panels (a) and (e), 125 MHz for panels (b) and (f), 250 MHz for panels (c) and (g), and 375 MHz for panels (d) and (h). The black curves show the probability of error of the gate operation while the red curves show the degree of rotation. The rotation angle corresponds to the definition of the gate $R_y(\theta) = \cos(\theta/2)\mathbb{1} + i\sin(\theta/2)\sigma_y$. The $\pi/4$ and $\pi/2$ points are explicitly indicated. For these simulations, a full master equation was used with appropriate relaxation and dephasing rates for both the electron and nuclear spins (detailed in the Appendix). The counter-rotating terms cause the rapid small oscillations.

single qubit rotation achieved in less than 10 ns by using four different pump strengths (62.5 MHz, 125 MHz, 250 MHz, and 375 MHz). At 62.5 MHz the hyperfine interaction is the primary cause of the error probability, as we have assumed that the nuclear spin is in an equal superposition state. Still for a $\pi/4$ rotation, the probability of error is approximately 0.0035. As we increase the driving-field strength, the error probability becomes dominated by the breakdown of the rotating wave approximation (the counter-rotating terms) and weak driving of the $|0\rangle_e \leftrightarrow |-1\rangle_e$ transition. The optimal working point (that minimizes both error sources) is a driving field around 125 MHz where an error probability of $\sim$0.002 is possible. For many quantum-information-processing tasks (computation or communication) this may not be low enough.

There are a number of ways to decrease this error probability. Remember that for the fastest gates we were beginning to populate the $|-1\rangle_e$ state. We can use a polarized drive field such that only the $|0\rangle_e \leftrightarrow |+1\rangle_e$ transitions is selected. This occurs for magnetic fields $B\gamma_e < D$. We plot the results of our simulations in Figs. 4(e)–4(h). In these cases we are looking at a two-level driven system which, however, is still subject to the rotating wave approximation and can break down if the driving amplitude is larger than the transition frequency. With a rotating wave approximation, $\nu = D + B\gamma_e$ and $\phi = -\pi$ the dynamics is governed by an effective Hamiltonian of the form

$$H \approx \hbar A_\parallel |+1\rangle_e\langle+1|_e I_z - \frac{\hbar\Omega_0}{2\sqrt{2}}(|0\rangle_e\langle+1|_e + |+1\rangle_e\langle 0|_e), \quad (9)$$

from which we can immediately confirm the intuition that the electron gates must operate much faster than the entangling gate time to avoid the hyperfine shift. That is,

$$A_\parallel \ll \frac{\Omega_0}{\sqrt{2}}. \quad (10)$$

The conditions imposed by Eqs. (8) and (10) imply an optimal drive frequency, which for a magnetic field of 50 mT is approximately $\frac{\Omega_0}{2\pi} \sim 250$ MHz as found by our numerical study. In such a case the x-rotation gate

$$R_e^x = \exp\left(i\frac{\Omega_0}{2\sqrt{2}}t[|0\rangle_e\langle+1|_e + |+1\rangle_e\langle 0|_e]\right) \quad (11)$$

follows trivially. Similarly, the y-rotation gate is produced when $\phi = -\pi/2$ is chosen. A comparison of the model with a numerical simulation of the system with appropriate decay probabilities is shown in Figs. 4(e)–4(h). With $\frac{\Omega_0}{2\pi} \sim 250$ MHz we can achieve a $\pi/4$ ($\pi/2$) rotation in approximately 1.5 ns (3 ns) with an error probability less than 0.0005 (0.001). These error probabilities are within what is typically required for large-scale quantum computation. The main cause of the loss in fidelity is associated with the $A_\parallel$ hyperfine interaction and the breakdown of the rotating wave approximation. If one requires even-higher-fidelity gates, one can use composite pulses to decouple the nuclear spin, but at the cost of slower gates.

The polarized microwave driving field (with ϕ variable) allows us to perform arbitrary x and y axis rotations, thus providing a mechanism to achieve the Pauli X and Y gates with high fidelity. Natural free evolution from $\hbar D|+1\rangle_e\langle+1|_e$ gives a z rotation but the time scale for the z rotation is fast and so good timing is necessary. Alternatively, it is likely to be better to perform z rotations as a combination of x and y. Combining these rotations allow the Pauli Z, S, and T gates to be achieved as well as the Hadamard H gate on the nanosecond timescale. Finally, combining such operations with the controlled-Z (CZ) entangling allows an arbitrary controlled unitary to be achieved with the nuclear spin as the control. In such cases, the overall gate time (with the nuclear spin as the control) is limited by the time to perform the CZ gate.

V. NUCLEAR ROTATIONS

The use of the nuclear spins either as a memory or as computational qubits has both advantages and disadvantages. First, the ^{15}N nuclear spin is spin half and so we do not need to worry about populating other energy levels when we drive it. Also, the comparative weakness of the nuclear gyromagnetic ratio provides isolation of the nucleus from electron rotations regardless of polarization. However, this comes at the cost of difficulty in affecting rotations on the nuclear-spin qubit without also affecting the electron spin. To avoid driving the electron spin, the time needed for nuclear gates will be much longer than for the entangling operation. However, this longer time means that the hyperfine interaction cannot be neglected during nuclear-spin rotations. The consequence of this is that the hyperfine shift leads to a driving frequency for the nucleus conditioned on the state of the electron, and that nuclear gates will need to be clocked on the entangling gate. This could also be an issue in other model systems for quantum computation. We can largely avoid this problem because nuclear rotations are only necessary upon initialization and measurement, which are both steps for which the electron is in a separable state and therefore can be manipulated with impunity.

The obvious choice of the electron state is the polarized ground state $|0\rangle_e$ where the electron and nuclear spins are effectively decoupled. The parallel hyperfine interaction imparts no additional phase between the two subsystems. In other words, while the frequency of the nuclear driving field is conditioned on the state of the electron ($A_\parallel \gg \Omega_0\gamma_n/\gamma_e$), we never need to consider this effect as the electron state remains the same. This argument, however, neglects thermalization effects on the electron spin which occurs at time scales around 0.25 s (for room temperature) or longer (for lower temperatures). With operation times around 50 μs it could be difficult to achieve high-fidelity operations.

In the $B\gamma_e < D$ regime, the Zeeman splitting of the nucleus is an order of magnitude smaller than the hyperfine splitting, which contributes to the $|+1\rangle_e|\downarrow\rangle_n \leftrightarrow |+1\rangle_e|\uparrow\rangle_n$ transition, but not the $|0\rangle_e|\downarrow\rangle_n \leftrightarrow |0\rangle_e|\uparrow\rangle_n$ transition. Hence, by initializing the electron spin in $|+1\rangle_e$, a larger driving field can be used before the rotating wave approximation on the nuclear rotation breaks down, implying a faster nuclear-rotation operation. For the nuclear spin, two processes are involved in the drive between the $|\uparrow\rangle_n$ and $|\downarrow\rangle_n$ states. There is obviously the direct driving shown in H_D, and the other is a second-order process involving the off-resonant drive on the electron and the perpendicular hyperfine term. Because the gyromagnetic ratio of the electron is large compared with that of the nucleus, this second-order term actually dominates at the magnetic field we have selected, which is necessary for useful nuclear-gate times. Operating in a regime where the state of the electron is unchanged by the drive field of frequency

$$\nu = A_\parallel - B\gamma_n + \frac{A_\perp^2}{2D + 2B\gamma_e}, \tag{12}$$

and where the perpendicular hyperfine term is off resonance, it is straightforward to show in our rotating frame that we perform a single-qubit nuclear rotation of the form

$$R_n^\phi = \exp\left(-i\frac{\Omega_0}{4}\left|\frac{A_\perp}{D + B\gamma_e} - \frac{\gamma_n}{\gamma_e}\right|\sigma_\phi^n t\right), \tag{13}$$

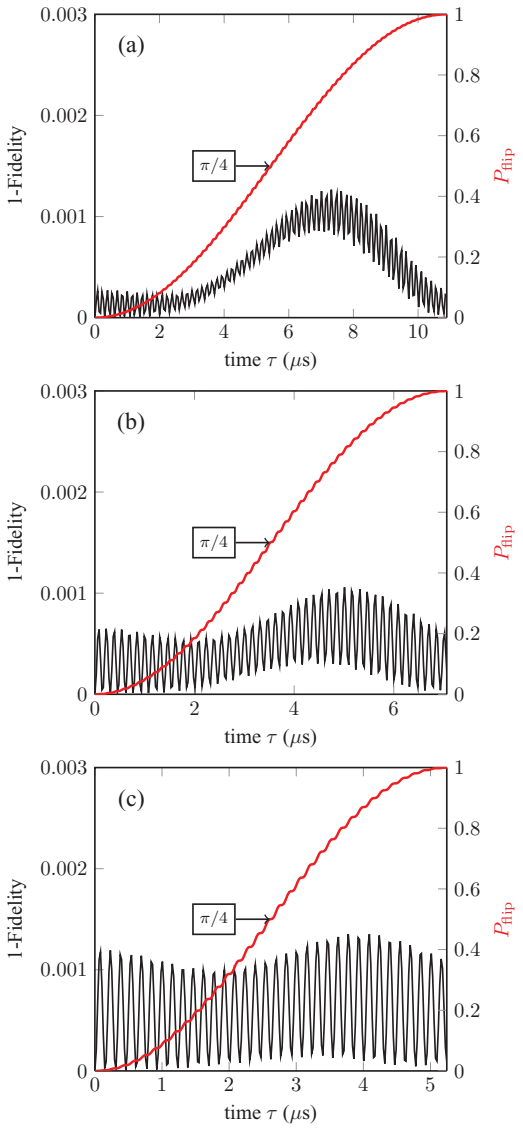

FIG. 5. (Color online) Simulation showing the fidelity for nuclear-spin rotations under both varying driving field and electron and nuclear-spin decoherence. The nuclear gate takes the longest to perform, and is thus most prone to error. We show three different driving field strengths: (a) 91 MHz, (b) 140 MHz, and (c) 189 MHz. The black curves show the probability of error of the gate operation while the red curves show the degree of rotation. The rotation angle corresponds to the definition of the gate of the form $R_y(\theta) = \cos(\theta/2)\mathbb{1} + i\sin(\theta/2)\sigma_y$. The $\pi/4$ points are explicitly indicated. For these simulations, a full master equation was used with appropriate relaxation and dephasing rates for both the electron and nuclear spins (detailed in the Appendix).

where $\sigma_0^n = \sigma_x^n$ and $\sigma_{-\pi/2}^n = \sigma_y^n$. The two terms in R_n^ϕ can be opposing such that, for a magnetic field $B = -0.9477$ T, no driving of the nuclear spin is possible due to destructive interference. Because we are working in the regimes $0 \leqslant B\gamma_e \leqslant D$, our gate is fastest for $B\gamma_e$ as small as possible. Now, as the nuclear gate takes a relatively long time to perform, it is the most sensitive to error. Figure 5 shows the results of a simulation of the nuclear-spin rotation for various driving fields when the electron spin is prepared in the $|+1\rangle_e$ state.

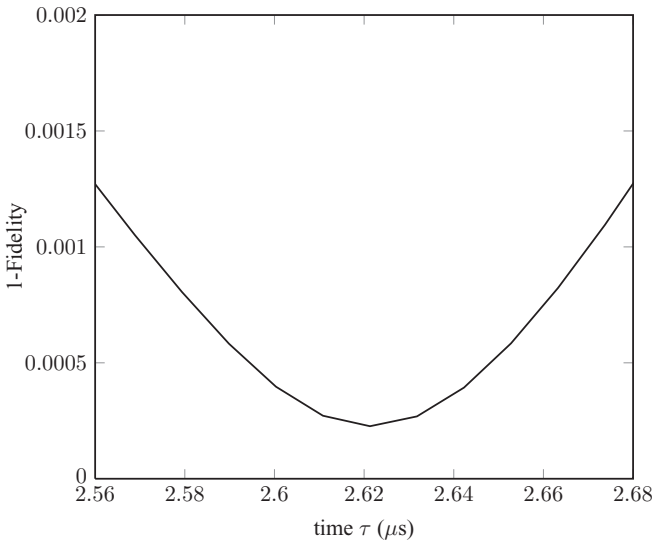

FIG. 6. Simulation showing the error probability $(1 - \langle +|_n \rho(t) |+\rangle_n)$ for nuclear-spin rotations under a 189 MHz driving field for a $\pi/4$ y rotation versus time.

For a driving field $\frac{\Omega_0}{2\pi} = 140$ MHz, the gate time required to rotate the nuclear spin from $|0\rangle_n$ to $|+\rangle_n$ is 3.54 μs with a error probability less than 0.001, as is shown in Fig. 5(b). This can be compared with a gate time of 57.8 μs for a similar rotation (but a slightly worse error probability of 0.003) if the electron spin was polarized in the $|0\rangle_e$ state. Our error estimate of 0.001 is also on the high side because we take a conservative estimate based on the maximum value of the oscillating curve at a given time rather than its minimum. The error probability can be reduced to below 0.0003 (see Fig. 6) just by accurately choosing the gate time to work at the minimum. In such a case our timing accuracy needs to be below 10 ns. By increasing the strength of the driving field, we can in principle achieve a $\pi/4$ rotation of 1 μs with error probability below 0.001. Such operations can be used to build the single-qubit-gate set required for quantum-information processing. However, for the generation of a cluster state, which is the core resource for most recent scalable quantum computational models, only the Hadamard H or $\sqrt{X}$ operation is required in general.

While we have been considering only the nuclear spin operations in this section, the electron spin could also be in a superposition state, thus allowing a CNOT between electron and nucleus, for instance, to be performed. However, there is a significant issue to be addressed before doing this; that is, when the electron spin is in a superposition state it dephases, and so it is difficult to achieve a gate operation with infidelity less than 0.001. This also highlights the necessity to carefully choose gates dependent on the properties of the physical system.

The results for both the electron- and nuclear-spin-gate operations as well as the hyperfine-mediated CZ gate show that such operations can be achieved under conditions with error probabilities of 0.001 or less [47]. Such error probabilities are generally required for quantum-information-processing tasks. To achieve the faster nuclear-spin rotations we need to polarize the electron spin in the $|+1\rangle_e$ state.

VI. GRAPH STATES

The creation of a two-qubit cluster state within a single NV center is straightforward given the set of operations we have. We begin with both the electron and nuclear spins prepared in their respective ground states. Then the nuclear spin is rotated to the $|+\rangle_n$ with the electron spin in the $|+1\rangle_e$ state. Once this has been completed the electron spin is then rotated to $|+\rangle_e$ and the natural CZ through the hyperfine interaction applied to create the cluster state $\frac{1}{2}(|0\rangle_e|0\rangle_n + |0\rangle_e|1\rangle_n + |+1\rangle_e|0\rangle_n - |+1\rangle_e|1\rangle_n)$. To extend it to a larger cluster state, we may consider doping with ^{13}C to add more qubits to couple to the electron spin. Alternatively, we could introduce a mechanism to entangle separated electron spins. The first would be experimentally easier; however, such an extension limits the size of the system. Furthermore, as the system becomes larger, the interaction will be more complicated and hence it is expected to be difficult to achieve high fidelity. To see this, a further detailed study is necessary for the dynamics of the multiqubit systems. The latter can be achieved using optical photons [28] and exhibits a good scaling nature, although it might look initially experimentally harder. In such a case the nuclear spins are again prepared in $|+\rangle_n$ state before the electron spins are entangled into a Bell state. Once this has been achieved the CZ gate is used to entangle the electron and nuclear spins—effectively creating a four-qubit cluster state. If required, a $\pi/4$ rotation of the electron spin followed by its measurement collapses the cluster state to a cluster between only the nuclear spins. In principle, this allows an arbitrary graph state to be generated between arbitrary nuclear spins [48]. Such states could be used for quantum-computation or -communication tasks.

VII. CIRCUITS AND IMPLEMENTATION

Before implementing quantum circuits, the NV^- center must be properly characterized. This can be done in a three-tiered way, starting with characterizing the electron spin, followed by the controlled-phase interaction, and finally the nuclear spin. For the electron spin, this is straightforward: Rabi oscillations can be measured optically [46] provided that the nucleus can be polarized to avoid interference from the hyperfine shift. Ultimately, once the characterization of a center is complete, the polarization of the nucleus should be done using a circuit to effectively swap its state with that of a polarized electron. However, for characterization purposes the exchange component of the hyperfine interaction can be used by preparing the electron in a polarized state and then sweeping the field over the exchange resonance. Circuits for characterizing the controlled-phase interaction and nuclear rotations are given in Fig. 7.

In the scenario of measurement-based quantum computation, only a few nontrivial quantum circuits are needed repetitively with a fully characterized system. Specifically, these are initialization of the nucleus, entangling of the electron and nucleus, and measuring of the nucleus via the electron. For initialization of the nucleus, it is clear that we must know the state of the nucleus or be able to project the nuclear spin into a known state, which relates itself to the measurement of the nuclear spin. In fact, the gates needed are applications

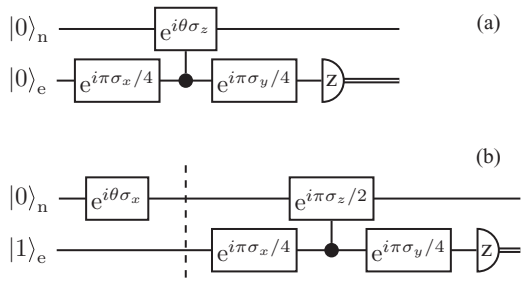

FIG. 7. Characterization of the hyperfine interaction. (a) By varying the time for which the hyperfine interaction is allowed to operate (the waiting time between x and y rotations on the electron) the probability of measuring the electron in $|0\rangle_e$ is $P_{|0\rangle} = \sin^2(\theta/2)$. (b) Characterization of the nuclear spin. By varying the input state of the nuclear spin and with a set waiting time between electron rotations, the probability of finding the electron in the $|0\rangle_e$ state is $P_{|0\rangle} = \sin^2(\theta)$. The dashed line is placed to emphasize that the nuclear rotation is performed only when the electron is in the $|1\rangle_e$ state, so that the splitting between the $|\uparrow\rangle_n$ and $|\downarrow\rangle_n$ states is enhanced by the hyperfine interaction (which is much larger than the magnetic splitting alone). This circuit can be employed to measure the state of the nucleus in the z basis.

of the two characterization circuits in Fig. 7 (characterization and use of electron rotations is considered trivial). By fixing the nuclear rotation angle and axis in the circuit in Fig. 7, the nuclear state can be measured in a particular basis. Application of this circuit, followed by a subsequent reset of the electron state into $|+1\rangle_e$ and a nuclear rotation qualifies as a preparation circuit for the nucleus. Application of the entangling gate consists of no more than a waiting time between single-qubit operations. With these operations and a probabilistic mechanism to entangle remote electron spins, we can then undertake various quantum communication and distributed quantum-computation tasks.

VIII. CONCLUDING DISCUSSION

In this paper, we have shown a universal set of operations which can be implemented in a NV^- center with a nitrogen-15 nucleus. The fastest operation is the electron-spin rotation, while the medium-term operation is the entangling gate which uses the hyperfine interaction. The electron-spin rotations can be done on timescale such that the nuclear spin is not affected. For the entangling gate, we utilize the controlled-phase interaction component rather than the exchange component of the hyperfine coupling. By sweeping the magnetic field, the exchange interaction can be turned on and off, making it useful for quantum-information processing. However, the controlled-phase interaction is always on and hence during the iSWAP operation there will be a contribution from the phase part which will need to be corrected. In addition, any imperfection in the iSWAP operation will lead to depopulation of the nuclear spin, opening up an error channel which will shorten the effective coherence time. Instead, a static field can be used that is far detuned from the exchange-interaction resonance to implement a highly efficient controlled-phase gate. This is preferable in terms of errors and stability coming from the static magnetic field. Finally, the longest-time operation is the nuclear-spin gate. This can be done by driving the nuclear spin weakly enough that we avoid disturbing the electron. In the case of cluster-state-based computation, the nuclear-spin rotation is typically required only twice, first at initialization and then just before prior to measurement. Hence the time necessary for this gate is not crucial as for the other gates. However, considering the potentially probabilistic nature of coupling two remote electron spins, it would be better to have as quick an operation as possible. Our numerical simulations show that we can achieve an error probability lower than the required fault-tolerant thresholds for a distributed quantum computer. These operations are done without the need for complicated composite sequences, which should significantly contribute to make the complexity in building larger scale NV^--center-based devices more manageable. It is now critical to re-emphasize that our results are based on operating temperatures between 4 and 80 K (and not room temperature). This is because we want our electron-spin relaxation time T_1 approximately 10^4 times greater than our longest gate operation (i.e., the nuclear-spin rotation), which takes a few microseconds to perform. It may be possible to engineer samples that operate at room temperature with this coherence properties. Finally, while the focus of this paper has been on NV^- centers with a nitrogen-15 nucleus, our results can be applied to many other solid-state systems.

ACKNOWLEDGMENTS

We acknowledge support from JSPS, the FIRST program, and NICT (A & B) in Japan.

APPENDIX A: THE INTERACTION PICTURE

For completeness it is necessary to define the interaction picture we are transforming into. The Hamiltonian for the electron-spin–nuclear-spin NV^--center hybrid system can be written as

$$H = H_0 + H_S + H_{HF} + H_D, \tag{A1}$$

where

$$H_0 = \hbar D S_z^2 + \hbar B\gamma_e S_z - \hbar B\gamma_n I_z, \tag{A2}$$

$$H_S = \hbar\frac{E}{2}(S_+^2 + S_-^2), \tag{A3}$$

$$H_{HF} = \hbar A_\parallel S_z I_z + \frac{1}{2}\hbar A_\perp (S_+ I_- + S_- I_+), \tag{A4}$$

$$H_D = \hbar\Omega_0 \cos(\omega t + \phi)\left(S_x - \frac{\gamma_n}{\gamma_e} I_x\right). \tag{A5}$$

For our purposes, it is convenient to move to an interaction picture defined by $\bar{H} = e^{iH_0 t/\hbar} H e^{-iH_0 t/\hbar} - H_0$. In such a situation Eq. (A1) simplifies to $\bar{H}_{\rm eff} = \bar{H}_S + \bar{H}_{HF} + \bar{H}_D$, where

$$\bar{H}_S = \hbar\, E|+1\rangle_e\langle -1|_e e^{i2B\gamma_e t} + \text{H.c.},$$

$$\bar{H}_{HF} = \hbar\, A_\parallel S_z I_z + \hbar\frac{A_\perp}{\sqrt{2}}[I_-|+1\rangle_e\langle 0|_e e^{i\Delta_+ t} + I_-|0\rangle_e\langle -1|_e e^{-i\Delta_- t} + \text{H.c.}],$$

$$\bar{H}_{\rm D} = \frac{\hbar\Omega_0}{\sqrt{2}}\cos(\nu t+\phi)\Big[|+1\rangle_{\rm e}\langle 0|_{\rm e}e^{i(D+B\gamma_{\rm e})t} + |0\rangle_{\rm e}\langle -1|_{\rm e}e^{-i(D-B\gamma_{\rm e})t} + \frac{\gamma_{\rm n}}{\sqrt{2}\gamma_{\rm e}}I_+e^{-iB\gamma_{\rm n}t}\Big] + {\rm H.c.},$$

with $\Delta_\pm = D \pm B\gamma_{\rm e} \pm B\gamma_{\rm n}$. The parallel term in $\bar{H}_{\rm HF}$ remains unchanged in this interaction picture since it commutes with H_0.

APPENDIX B: RESONANCES AND THE STRAIN-INDUCED SPLITTING

The strain-induced splitting from our Hamiltonian causes the population to oscillate between the $|+1\rangle_{\rm e}$ and $|-1\rangle_{\rm e}$ electron-spin states. If the energy difference between these states is quite small, then the population may move completely from one state to the other. In our system the $|-1\rangle_{\rm e}$ state is outside of the computational basis, and so we want to avoid the action of strain-induced splitting. We can derive the width and position of this resonances with respect to the applied magnetic field along the NV^- axis. Starting with Eq. (A1), we will neglect the driving term and the perpendicular hyperfine term (the perpendicular hyperfine term is far from resonance with the low magnetic fields considered here). In addition, the strain-induced splitting does not involve the $|0\rangle_{\rm e}$ state, so we may disregard this state for the moment. We are this left with the reduced Hamiltonian

$$H = \hbar B\gamma_{\rm e}S_z - \hbar B\gamma_{\rm n}I_z + \hbar A_\parallel S_zI_z + \hbar\frac{E}{2}(S_+S_+ + S_-S_-).$$

There are two resonances which are dependent on the state of the nucleus through the parallel hyperfine term and the nuclear magnetic term:

$$H_{|\uparrow\rangle_{\rm n}} = \hbar B\gamma_{\rm e}S_z + \hbar\frac{A_\parallel}{2}S_z + \hbar\frac{E}{2}(S_+S_+ + S_-S_-),$$
$$H_{|\downarrow\rangle_{\rm n}} = \hbar B\gamma_{\rm e}S_z - \hbar\frac{A_\parallel}{2}S_z + \hbar\frac{E}{2}(S_+S_+ + S_-S_-).$$

Selecting the nucleus in the $|\uparrow\rangle_{\rm n}$ state, the resultant 2×2 Hamiltonian has equal diagonal terms when $B = -A_\parallel/2\gamma_{\rm e}$ and $B = +A_\parallel/2\gamma_{\rm e}$ when the nucleus is in the $|\downarrow\rangle_{\rm n}$ state, giving us the resonances at ∓ 0.054 mT. Taking the hyperfine terms into account leads to a shift of these resonances by $\approx 4.6\ \mu$T. Again assuming that the perpendicular hyperfine interaction may safely be neglected, the resonances have Lorentzian profiles of $B_{\rm FWHM} = 2E/\gamma_{\rm e}$. For a strain-induced splitting of the order $E \sim 1$ MHz our chosen magnetic field of $B = 50$ mT is safely distant from these resonances.

APPENDIX C: RESONANCES AND THE HYPERFINE COUPLING

When a electron transition is close in frequency to the nuclear transition, an excitation may oscillate between them. In isolation, the perpendicular hyperfine interaction provides an iSWAP gate, which is entangling. However, the exchange interaction is not in isolation due to the parallel hyperfine term in the Hamiltonian, which may not be tuned to be negligible. In addition, tuning the exchange interaction increases the complexity of the gate, as it would require the fine control of a strong magnetic field. An added incentive to avoid an exchange interaction is the impact that errors in the interaction would have on the large-scale system. This interaction was recently demonstrated as a quantum memory [20], for which the nucleus is initially polarized and iSWAP and SWAP are the same up to a global phase. It is conceivable that the inverse operation could be used to initialize the nuclear state by tuning the exchange interaction into resonance and polarizing the electron [21]. This offers a potential alternative to the initialization and readout operations that we describe in Sec. VII.

APPENDIX D: MASTER EQUATION AND NUMERICAL SIMULATIONS

We need to be able to model the various electron-spin and nuclear-spin rotations as well the controlled Z gate, including the effects of decoherence (thermalization) and dephasing on both the electron and nuclear spins. This can be achieved using the master equation

$$\begin{aligned}\frac{\partial\bar{\rho}}{\partial t} = &-\frac{i}{\hbar}[\bar{H}_{\rm eff},\bar{\rho}] + \Gamma_n^{(2)}(\sigma_z\bar{\rho}\sigma_z - \bar{\rho})\\ &+ \frac{\Gamma_e^{(1)}(\bar{n}_e+1)}{2}(2S_-\bar{\rho}S_+ - S_+S_-\bar{\rho} - \bar{\rho}S_+S_-)\\ &+ \frac{\Gamma_e^{(1)}\bar{n}_e}{2}(2S_+\bar{\rho}S_- - S_-S_+\bar{\rho} - \bar{\rho}S_-S_+)\\ &+ \frac{\Gamma_n^{(1)}(\bar{n}_n+1)}{2}(2\sigma_-\bar{\rho}\sigma_+ - \sigma_+\sigma_-\bar{\rho} - \bar{\rho}\sigma_+\sigma_-)\\ &+ \frac{\Gamma_n^{(1)}\bar{n}_n}{2}(2\sigma_+\bar{\rho}\sigma_- - \sigma_-\sigma_+\bar{\rho} - \bar{\rho}\sigma_-\sigma_+),\end{aligned} \tag{D1}$$

where $\Gamma_e^{(1)}$ is the decoherence rate of the electron spin (T_1 related), $\Gamma_n^{(1)}$ is the decoherence rate of the nuclear spin (T_1 related), and $\Gamma_n^{(2)}$ is the dephasing of the nuclear spin (T_2^* related). $S_\pm$ are the usual raising and lower operators of the electron while $\sigma_\pm$ are the raising and lower operators of the nuclear spin. $\bar{n}_e$ ($\bar{n}_n$) is the mean photon number of the electron-spin (nuclear-spin) bath at a temperature T.

The electron spin also has a dephasing effect, but this cannot be modelled by a master equation term of the form $S_z\bar{\rho}S_z - \bar{\rho}$ because the spin bath comes from low-frequency noise. Low-frequency noise can be modelled in a slightly different way by considering adding an extra Hamiltonian of the field $H = \lambda f(t)S_z$ to $\bar{H}_{\rm eff}$ where λ is the coupling strength and $f(t)$ is a symmetric classical normalized Gaussian noise function.

The overall master equation can be numerically solved by using standard techniques and the required fidelities of the operations calculated.

[1] T. D. Ladd, F. Jelezko, R. Laflamme, Y. Nakamura, C. Monroe, and J. L. O'Brien, Nature (London) **464**, 45 (2010).

[2] S. E. Coe and R. S. Sussmann, Diamond Relat. Mater. **9**, 1726 (2000).

[3] B. Lux and R. Haubner, Ceram. Int. **22**, 347 (1996).

[4] A. M. Zaitsev, *Optical Properties of Diamond: A Data Handbook*, 1st ed. (Springer, Berlin, 2001).

[5] G. Davies and M. F. Hamer, Proc. R. Soc. London, Ser. A **348**, 285 (1976).

[6] R. T. Harley, M. J. Henderson, and R. M. Macfarlane, J. Phys. C: Solid State Phys. **17**, L233 (2000).

[7] N. R. S. Reddy, N. B. Manson, and E. R. Krausz, J. Lumin. **38**, 46 (1987).

[8] A. D. Greentree, P. Olivero, M. Draganski, E. Trajkov, J. R. Rabeau, P. Reichart, B. C. Gibson, S. Rubanov, S. T. Huntington, D. N. Jamieson, and S. Prawer, J. Phys.: Condens. Matter **18**, S825 (2006).

[9] G. Balasubramanian, I. Y. Chan, R. Kolesov, M. Al-Hmoud, J. Tisler, C. Shin, C. Kim, A. Wojcik, P. R. Hemmer, A. Krueger, T. Hanke, A. Leitenstorfer, R. Bratschitsch, F. Jelezko, and J. Wrachtrup, Nature (London) **455**, 648 (2008).

[10] J. R. Maze, P. L. Stanwix, J. S. Hodges, S. Hong, J. M. Taylor, P. Cappellaro, L. Jiang, M. V. G. Dutt, E. Togan, A. S. Zibrov, A. Yacoby, R. L. Walsworth, and M. D. Lukin, Nature (London) **455**, 644 (2008).

[11] G. Balasubramanian, P. Neumann, D. Twitchen, M. Markham, R. Kolesov, N. Mizuochi, J. Isoya, J. Achard, J. Beck, J. Tissler, V. Jacques, P. R. Hemmer, F. Jelezko, and J. Wrachtrup, Nat. Mater. **8**, 383 (2009).

[12] V. M. Acosta, E. Bauch, M. P. Ledbetter, C. Santori, K. M. C. Fu, P. E. Barclay, R. G. Beausoleil, H. Linget, J. F. Roch, F. Treussart, S. Chemerisov, W. Gawlik, and D. Budker, Phys. Rev. B **80**, 115202 (2009).

[13] P. H. Chung, E. Perevedentseva, J. S. Tu, C. C. Chang, and C. L. Cheng, Diamond Relat. Mater. **15**, 622 (2006).

[14] C.-C. Fu, H.-Y. Lee, K. Chen, T.-S. Lim, H.-Y. Wu, P.-K. Lin, P.-K. Wei, P.-H. Tsao, H.-C. Chang, and W. Fann, Proc. Natl. Acad. Sci. USA **104**, 727 (2007).

[15] J.-I. Chao, E. Perevedentseva, P.-H. Chung, K.-K. Liu, C.-Y. Cheng, C.-C. Chang, and C.-L. Cheng, Biophys. J. **93**, 2199 (2007).

[16] F. Neugart, A. Zappe, F. Jelezko, C. Tietz, J. P. Boudou, A. Krueger, and J. Wrachtrup, Nano Lett. **7**, 3588 (2007).

[17] A. Beveratos, S. Kühn, R. Brouri, T. Gacoin, J. P. Poizat, and P. Grangier, Eur. Phys. J. D **18**, 191 (2002).

[18] A. Beveratos, R. Brouri, T. Gacoin, A. Villing, J. P. Poizat, and P. Grangier, Phys. Rev. Lett. **89**, 187901 (2002).

[19] F. Jelezko, T. Gaebel, I. Popa, A. Gruber, and J. Wrachtrup, Phys. Rev. Lett. **92**, 076401 (2004).

[20] G. D. Fuchs, G. Burkard, P. V. Klimov, and D. D. Awschalom, Nat. Phys. **7**, 789 (2011).

[21] B. Smeltzer, J. McIntyre, and L. Childress, Phys. Rev. A **80**, 050302(R) (2009).

[22] M. V. G. Durr, L. Childress, L. Jiang, E. Togan, J. Maze, F. Jelezho, A. S. Zibrov, P. R. Hemmer, and M. D. Lukin, Science **316**, 1312 (2007).

[23] L. Jiang, J. S. Hodges, J. R. Maze, P. Maurer, J. M. Taylor, D. G. Cory, P. R. Hemmer, R. L. Walsworth, A. Yacoby, A. S. Zibrov, and M. D. Lukin, Science **326**, 267 (2009).

[24] P. Neumann, J. Beck, M. Steiner, F. Rempp, H. Fedder, P. R. Hemmer, J. Wrachtrup, and F. Jelezho, Science **329**, 542 (2010).

[25] L. Robledo, L. Childress, H. Bernien, B. Hensen, F. A. Alkemade, and R. Hanson, Nature (London) **477**, 574 (2011).

[26] L. Childress, M. V. Gurudev Dutt, J. M. Taylor, A. Zibrov, F. Jelezko, J. Wrachtrup, P. R. Hemmer, and M. D. Lukin, Science **314**, 281 (2006).

[27] H. Bernien, L. Childress, L. Robledo, M. Markham, D. Twitchen, and R. Hanson, Phys. Rev. Lett. **108**, 043604 (2012).

[28] H. Bernien, B. Hensen, W. Pfaff, G. Koolstra, M. S. Blok, L. Robledo, T. H. Taminiau, M. Markham, D. J. Twitchen, L. Childress, and R. Hanson, Nature (London) **497**, 86 (2013).

[29] L. I. Childress, J. M. Taylor, A. S. Sørensen, and M. D. Lukin, Phys. Rev. A **72**, 052330 (2005).

[30] L. Childress, J. M. Taylor, A. S. Sørensen, and M. D. Lukin, Phys. Rev. Lett. **96**, 070504 (2006).

[31] S. C. Benjamin, D. E. Browne, J. Fitzsimons, and J. J. L. Morton, New J. Phys. **8**, 141 (2006).

[32] L. Jiang, J. M. Taylor, A. S. Sørensen, and M. D. Lukin, Phys. Rev. A **76**, 062323 (2007).

[33] S. D. Barrett and P. Kok, Phys. Rev. A **71**, 060310 (2005).

[34] T. van der Sar, Z. H. Wang, M. S. Blok, H. Bernien, T. H. Taminiau, D. M. Toyli, D. A. Lidar, D. D. Awschalom, R. Hanson, and V. V. Dobrovitski, Nature (London) **484**, 82 (2012).

[35] R. Raussendorf, J. Harrington, and K. Goyal, Ann. Phys. (NY) **321**, 2242 (2006).

[36] While magnetic field manipulation is possible, it is difficult to achieve with really high fidelity.

[37] S. Felton, A. M. Edmonds, M. E. Newton, P. M. Martineau, D. Fisher, D. J. Twitchen, and J. M. Baker, Phys. Rev. B **79**, 075203 (2009).

[38] Because we are operating with a magnetic field at $B = 50$ mT we are far detuned from these resonances and so will be operating again in the dispersive regime.

[39] A. Jarmola, V. M. Acosta, K. Jensen, S. Chemerisov, and D. Budker, Phys. Rev. Lett. **108**, 197601 (2012).

[40] T. Ishikawa, K.-M. C. Fu, C. Santori, V. M. Acosta, R. G. Beausoleil, H. Watanabe, S. Shikata, and K. M. Itoh, Nano Lett. **12**, 2083 (2012).

[41] K. Fang, V. M. Acosta, C. Santori, Z. Huang, K. M. Itoh, H. Watanabe, S. Shikata, and R. G. Beausoleil, Phys. Rev. Lett. **110**, 130802 (2013).

[42] N. Bar-Gill, L. M. Pham, A. Jarmola, D. Budker, and R. L. Walsworth, Nat. Commun. **4**, 1743 (2013).

[43] P. C. Maurer, G. Kucsko, C. Latta, L. Jiang, N. Y. Yao, S. D. Bennett, F. Pastawsk, D. Hunger, N. Chisholm, M. Markham, D. J. Twitchen, J. I. Cirac, and M. D. Lukin, Science **336**, 1283 (2012).

[44] B. W. Shore, Phys. Rev. A **24**, 1413 (1981).

[45] Assuming both our electron and nuclear spin has been initialized in their grounds states $|0\rangle_e|0\rangle_n$, the separable state $|+\rangle_e|+\rangle_n$ can be created as follows: We begin by first rotating the electron spin from $|0\rangle_e \rightarrow |+1\rangle_e$. A nuclear-spin rotation is then performed (detailed in the main text), rotating $|0\rangle_n \rightarrow |+\rangle_n$. Because the electron spin is in the $|+1\rangle_e$ state, it does not experience dephasing. Once the nuclear-spin operation is complete, an electron-spin rotation takes $|+1\rangle_e \rightarrow |+\rangle_e$.

[46] G. D. Fuchs, V. V. Dobrovitski, D. M. Toyli, F. J. Heremans, and D. D. Awschalom, Science **326**, 1520 (2009).

[47] The technique used to perform the nuclear-spin rotations can also be used to perform controlled nuclear-spin rotations. For

instance, if we prepare the electron spin in the $\frac{1}{\sqrt{2}}[|0\rangle_e + |+1\rangle_e]$ with the nuclear spin in the $|0\rangle_n$ state. Applying a drive field of frequency $\nu = A_\parallel - B\gamma_n + \frac{A_\perp^2}{2D+2B\gamma_e}$ for a time t such that $\frac{\Omega_0}{4}|\frac{A_\perp}{D+B\gamma_e} - \frac{\gamma_n}{\gamma_e}|t = \pi/2$ will result in an entangled state of the form $\frac{1}{\sqrt{2}}[|0\rangle_e|0\rangle_n + e^{iA_\parallel t}|+1\rangle_e|1\rangle_n]$. The phase factor can in principle be easily removed; however, we do have an issue associated with T_2^* of the electron spin and the time to perform the gate. The time to perform the gate is on the order of 7μs while $T_2^* \sim 90\mu$s. Without composite pulses sequences to enhance this coherence time, we would have an extra intrinsic loss in fidelity of approximately 0.003.

[48] K. Nemoto, M. Trupke, S. J. Devitt, A. M. Stephens, K. Buczak, T. Nobauer, M. S. Everitt, J. Schmiedmayer, and W. J. Munro, arXiv:1309.4277.